This is the accepted version of the publication Chen L, Choy YS, Wang TG, Chiang YK. Fault detection of wheel in wheel/rail system using kurtosis beamforming method. Structural Health Monitoring. 2020;19(2):495-509. Copyright © 2019 The Author(s). DOI: 10.1177/1475921719855444.

Fault detection of wheel in wheel/rail system using kurtosis beamforming method

CHEN Long[1], CHOY Yat Sze*[1], WANG Tian Gang[2], CHIANG Yan Kei[1]

[1] Department of Mechanical Engineering, The Hong Kong Polytechnic University. 11 Yuk Choi Rd, 999077, Hong Kong

[2] China Academy of Space Technology. No.104 Youyi Rd. Haidian District. Beijing. China

*Corresponding author.

E-mail address: mmyschoy@polyu.edu.hk

Abstract

Fault detection systems are typically applied in the railway industry to examine the structural health status of the wheel/rail system. We herein propose a time-domain kurtosis beamforming technique using an array of microphones for the fault identification and localisation of the wheel/rail system under an environment with high background noise. As an acoustics-based noncontact diagnosis method, this technique overcomes the challenge of the contact between the sensors and examined structures, and it is more applicable for impulsive signals of broadband nature, such as impact noise generated from faults on the wheel surface. Moreover, the application of kurtosis enables the identification and localisation at low signal-to-noise ratio. Under such circumstance the impulsive signals generated by faults were totally merged in rolling noise and background noise. Meanwhile, different types of faults on the wheels could be identified and localised by observing the kurtosis value on the beamforming sound map. The effectiveness of the proposed method to diagnose the type of wheel fault with low signal-to-noise ratio and moving source has been validated experimentally. This method may provide a useful tool for the routine maintenance of trains.

Keywords: array signal processing; time-domain beamforming; impulsive signal; kurtosis; wheel-rail contact.

1. Introduction

Fault diagnosis in rotating machinery is crucial for conditional-based maintenance in several applications such as those in the railway industry, escalators, and bearings and gears in machines. Currently, approximately 21,000 locomotives, 73,000 carriages, and 799,000 wagons are operational in China. Structural condition monitoring systems are widely implemented in the railway industry and various monitoring approaches have been proposed for the inspection of wheel and rail conditions. However, nearly half of the train accidents were the result of imperfect train wheels owing to the prolonged usage of the wheel/rail system[1], and the comprehensive maintenance cost of checking all the wheels can be expensive. To rectify such situations, we propose a time-domain kurtosis beamforming technique using an array of microphones for fault identification and localisation of the wheel/rail system.

Wheels wear out or get damaged due to frequent use, leading to an uneven surface or an irregular shape. Rolling noise ensues when wheels pass over the rail. This is predominantly caused by undulations of the wheel and the surface of the rail, thereby inducing a vertical relative vibration. Impact noise can be considered as an extreme form of rolling noise, which is caused by faulty or uneven structural surfaces of the wheel or rail. Contrary to the traditional acoustics emission (AE) phenomenon, impact noise is an impulsive, short duration pressure pulse with a peak amplitude that is much higher than that of the rolling noise. It is a quasi-periodic series of impulsive signal according to the cycle of the rotating wheel[2]. Broadband, short duration, low acoustic energy level, low signal-to-noise ratio (SNR), and quasi-periodical nonstationary characteristics are some of the features of impact noise[3]. In the wheel/rail system, faults or imperfections can be categorised into wheel-flat due to severe wearing, dent due to crack, and squat due to rolling contact fatigue[4-8]. It is critical to identify and localise the position of the fault on the wheel so that repair and maintenance can be performed on time. However, it remains technically challenging to localise the wheel fault in real time.

In order to implement a reliable structural condition monitoring system, a variety of fault detection methods have been developed, such as vibration analysis, magnetic testing, Lamb wave analysis, and acoustic emission (AE)[9-15]. In vibration analysis, the presence of defects is identified by observing the frequency shift or variation of the pattern of the time-variant signal and comparing that

with the patters obtained from a healthy structure[1]. In magnetic testing, electromagnetic acoustic transducer (EMAT) probes are mounted along the rails to inspect the wheels when a train passes by in a short time. The Rayleigh wave is transmitted when the wheel is contact with the EMAT probe. The Rayleigh wave pulse makes several round trips along the tread of the wheel. The EMAT probes detect echoes from discontinuities in the tread in the pulse echo mode after these round trips[16]. Lamb waves are generated and captured by piezoelectric sensors and possess high susceptibility to interference on a propagation path. These are considered cost effective for fault identification, compared to the previous two techniques. Different types of faults and damages in the structure can be identified by selecting the appropriate Lamb modes[12]. AE is a phenomenon, wherein a radiation of transient elastic waves are generated from a rapid release of strain energy resulting from deformation or damage within or on the surface of a material. These waves are generated by the interaction of two media in relative motion and an AE signal is emitted only at the time of these events[10]. In practical applications, several AE sensors are mounted on the wheel and techniques such as rail testing model, wavelet transform (WT) and Shannon entropy are utilized to filter the AE signal and detect the defects based on the feature of time window. The Shannon entropy of noise signals has lower fluctuation and smaller standard deviation than the AE signals so that defects in rails can be detected[17]. This method provides satisfactory performance under an environment of high background noise. However, the influence of noise effects on fault detection is significant, when the train travels in high speeds. Furthermore, the AE method can only monitor the generation of faults in a structural health monitoring system. It is not used to detect the structural defeats after the formation of faults.

These aforementioned fault detection approaches, can mostly be regarded as contact methods, as the sensors are required to be mounted on the surface of the structure with wiring. In order to eliminate the additional loading by the sensor on the structure or any further issue related to the moving structure, coupling and real-time diagnostic need in railway industry, a noncontact measurement approach, such as acoustics-based diagnosis, is a more attractive option. Some researchers have strived to employ acoustic-based diagnosis (ABD) methods to detect faults in rotating machinery. This includes utilising the symmetrised dot pattern (SDP) method to detect abnormalities in bearings, and the near-field holography (NAH) technique to detect faults in a gear box[18, 19]. However, for the NAH technique, an array of microphones should be located close to the detecting surface, which can be difficult to achieve. Therefore, an alternative method, called beamforming technique, is used to detect the structural

damages. By exploiting the different time-series characteristics, time-domain methods can be used to attain statistical decisions for fault detection and identification[20]. Time-domain beamforming is considered effective and accurate to localise moving, transient, or broadband sound sources[21, 22]. Time-domain beamformer can be evaluated by peak value, root mean square (RMS) value[23], or kurtosis. Among these three estimators, kurtosis is considered the best indicator of signal impulsiveness for fault detection of rotating components[24]. A team of researchers used the beamforming spectral kurtosis (SK) in the frequency domain to detect the fault of each component in a complex rotating machinery system[25, 26]. The impact signal generated by a wheel with uneven structural surface possesses the broad frequency feature. It is difficult to identify the appropriate frequency bands for calculating the SK of a broadband signal. Subsequently, the research findings indicate that the wheel faults can hardly be identified using the frequency-domain method. Therefore, this paper attempts to achieve fault visualisation as a function of time and space, instead of frequency and space. The objectives of this study are to (1) localise and identify the faults of a wheel in an environment with different SNRs using time-domain kurtosis beamformer, (2) obtain corresponding kurtosis values for different types of wheel faults, which are helpful for differentiating the types of faults occurring during the early stages, (3) study the accuracy of fault detection under different SNRs and durations of data acquisition, and (4) show the possibility of detecting faults on a moving train.

2. Methodologies

2.1 Time-domain beamforming

Fig. 1 illustrates a spherical wavefront from a point source incident to a linear array of M microphones. The sound signals received at the microphone array can be expressed as

$$\mathbf{p}(t) = [p_1(t) \quad p_2(t) \quad \cdots \quad p_M(t)]^T \tag{1}$$

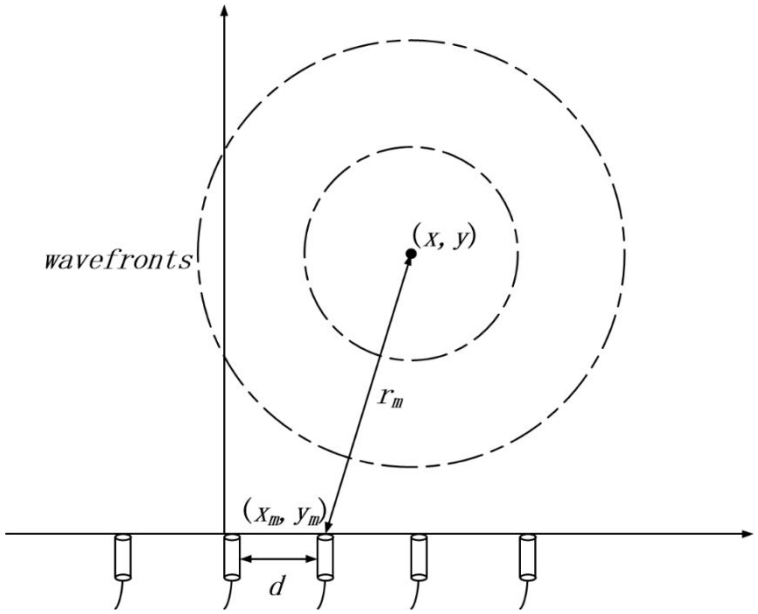

Fig. 1. The general time-domain beamforming system (spherical wavefront model).

An intentional time delay is applied to each measured signal in $\mathbf{p}(t)$ such that the time difference is compensated. The beamformer output can be derived by adding all the delayed signals. In the near-field assumption, the time-domain delay-and-sum (DAS) beamformer output with respect to the positional parameter r_m can be defined as

$$b(r_m,t)=\frac{1}{M}\sum_{m=1}^{M}p_m(t-\frac{r_m}{c}) \tag{2}$$

in which c is the representative sound speed, and $r_m(x_m,y_m)=\sqrt{(x-x_m)^2+(y-y_m)^2}$ is the distance between the sound source *(x, y)* and the *m*th microphone in array *(x_m, y_m)*, and m is the index of each microphone (m=1, …, M). As the time-domain beamforming output $b(r_m,t)$ is a function of time and space, it can emphasise the temporal characteristics of the source signal. The corresponding beamforming power can be expressed as

$$\beta(r_m)=E[\left|b(r_m,t)\right|^2] \tag{3}$$

in which E represents the expectation operator.

For the moving sound signal whose position in the sound field (as shown in Fig. 2) is continuously changing with respect to time τ, two primary distortions in the time domain should be considered in the localisation approach: the arrival time of the sound signal, and the Doppler amplification. For a linear motion with speed v_0, the measured sound pressure at the observation position $\mathbf{r}=[x,y,z]$ is given by

$$p(\mathbf{r},t)=\frac{q_0(\tau)}{4\pi|\mathbf{r}-\mathbf{r}_0(\tau)|}\frac{1}{|1-M_0(\tau)|} \tag{4}$$

in which q_0 is the time signal, $\mathbf{r}_0=[v_0\tau_j,0,0]$ is the position of source, and M_0 is the Mach number term:

$$M_0(\tau)=\frac{v_0}{c}\frac{x-v_0\tau}{\sqrt{(x-v_0\tau)^2+y^2+z^2}} \tag{5}$$

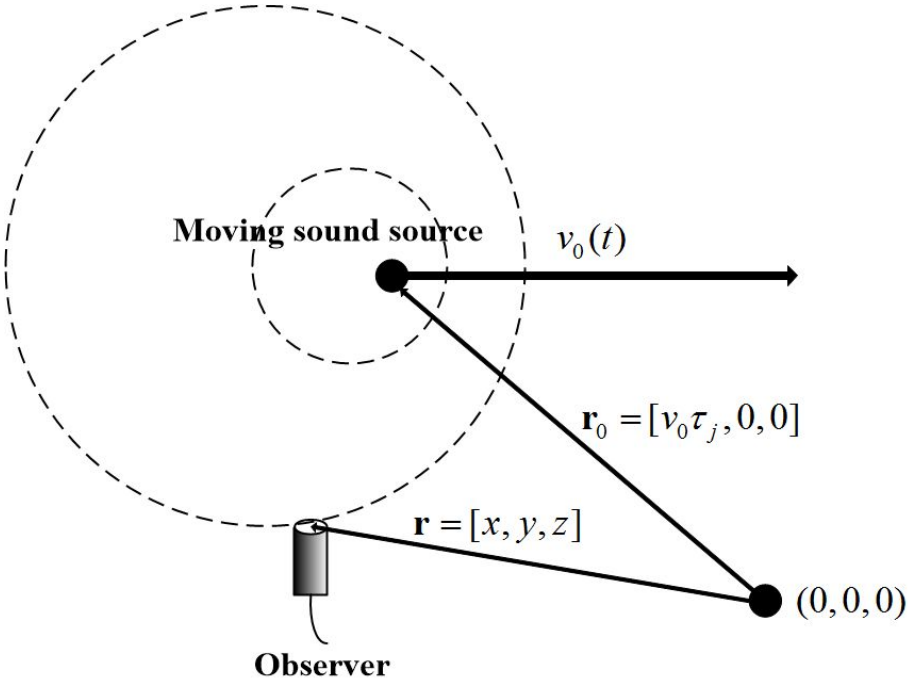

Fig. 2. Propagation wavefront produced by a moving sound source.

To neutralise the distortion of the Doppler amplification, a method called de-Dopplerisation[27] can be adopted in the beamforming localisation approach. Using eq. (4), the source signal can be re-arranged as:

$$q_0(\tau) = 4\pi \left|\mathbf{r} - \mathbf{r}_0(\tau)\right| \left|1 - M_0(\tau)\right| p(\mathbf{r}, \tau + \frac{\left|\mathbf{r} - \mathbf{r}_0(\tau)\right|}{c}) \tag{6}$$

in which the sound pressure is assumed to be measured by a fixed microphone array.

Assuming that κ source signals are on a moving frame with a centre $\mathbf{r}_0(\tau)$ as shown in Fig. 3, and the speed v_0 is estimated by m microphones, each position of the source signals can be expressed as $\mathbf{r}_0(\tau) + \Delta\mathbf{r}_\kappa$ (κ=1,L ,K), and the de-Dopplerised time-domain beamforming output can be written as

$$b(\Delta\mathbf{r}_\kappa, \tau) = \frac{1}{M} \sum_{m=1}^{M} 4\pi \left|\mathbf{r}_m - \left[\mathbf{r}_0(\tau) + \Delta\mathbf{r}_\kappa\right]\right| \left|1 - \frac{\left|v_0(\tau)\right|}{c} \cos\varphi_{m\kappa}(\tau)\right| p(\mathbf{r}_m, \frac{\tau + \left|\mathbf{r}_m - \left[\mathbf{r}_0(\tau) + \Delta\mathbf{r}_\kappa\right]\right|}{c}) \tag{7}$$

in which c is the speed of sound, $\mathbf{r}_m$ is the position of the mth microphone, and $\cos\varphi_{m\kappa}(\tau)$ is the angle between the directions of $\mathbf{v}_0$ and $\mathbf{r}_m - \left[\mathbf{r}_0(\tau) + \Delta\mathbf{r}_\kappa\right]$.

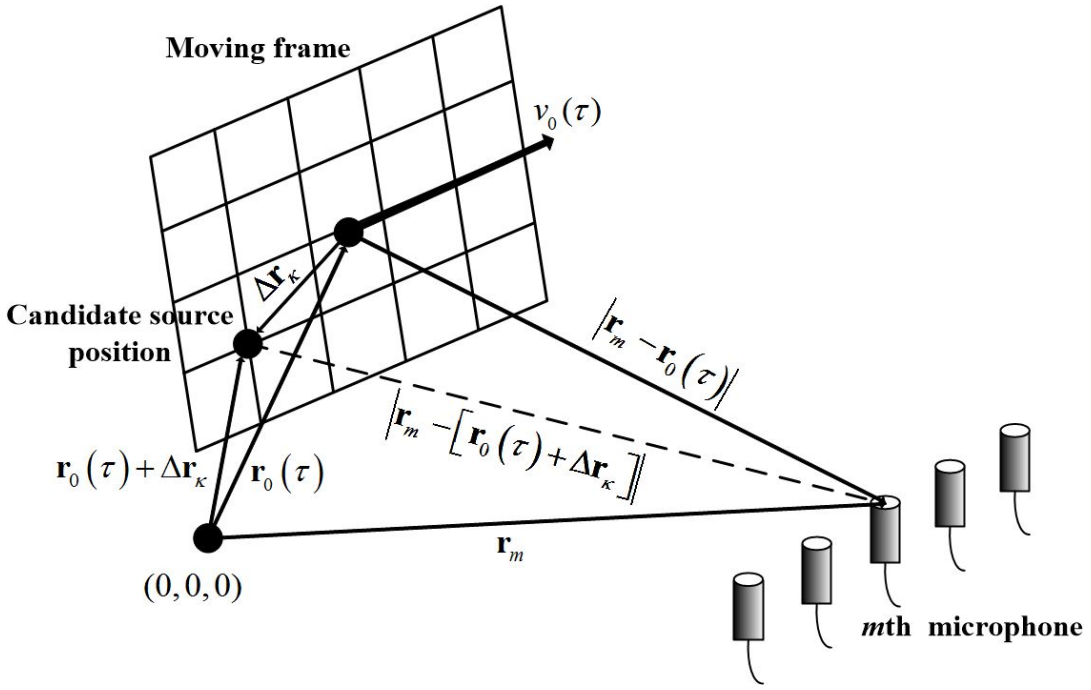

Fig. 3. De-Dopplerisation beamforming approach with sound source on a moving frame.

2.2 Time-domain beamforming integrated with kurtosis.

Herein, a fault detection and localisation strategy is established by integrating the time-domain

beamforming technique with kurtosis. The kurtosis is the fourth standardised moment, defined as

$$Kurt(x) = \frac{E\{[x - \mu(x)]^4\}}{[\sigma(x)]^4} \tag{8}$$

in which $\mu(x)$ is the mean value of x, $\sigma(x)$ is the standard deviation of x, and E represents the expected value of the quantity. The normal distribution has a kurtosis value of 3, and -3 is often used such that the normal distribution has a kurtosis value of zero. In statistics, kurtosis is a measure of the peakedness of a variable. A higher kurtosis value of a signal is the result of its larger deviations in the time history.

Three different typical signals were generated, and their kurtosis values were compared in Table 1. The rectangular wave and sine wave are typical low kurtosis distributions. The deviations of their time history were less than the normal distribution. Similar to other univariate normal distributions, the kurtosis value of white noise is 3. The impulsive signal was adopted to imitate the impact noise generated by the imperfections of rotating mechanisms. Further, its kurtosis value was extremely higher than those of the rectangular wave, sine wave, or white noise.

Table 1

Different signals and their kurtosis values.

Type of signal	Kurtosis value
Rectangular wave	1.000
Sine wave	1.500
White noise	3.0280
Gaussian impulses	98.5976

The kurtosis of the beamformer, which is named kurtosis beamformer, is as follows:

$$Kurt(r_m) = \frac{E\left(\left\{b(r_m,t) - \mu\left[b(r_m,t)\right]\right\}^4\right)}{\left\{\sigma\left[b(r_m,t)\right]\right\}^4} \tag{9}$$

It is noteworthy that unlike the conventional beamforming power, the kurtosis beamformer in the current study is dimensionless.

3. Experimental study

3.1 The roller test rig

To simulate the real wheel/rail system, a rotating machinery system was designed and constructed as shown in Fig. 4. The system was composed of two rollers and two different shafts. One shaft of diameter 25 mm was coupled with a cast iron wheel of diameter 200 mm that served as the rail, and one shaft of diameter 20 mm also was coupled with a cast iron wheel of diameter 150 mm that served as the wheel. Both shafts were driven by 60 W/220 V direct current (DC) motors (5IK60RGU-CF) with decelerators (5GU-3K). Belt transmission and universal coupling were applied to the roller test rig to ensure that the motion of the wheel with wheel-flat possessed enough space. The different speeds of the two shafts could be achieved by speed control switches that were attached with DC motors and an optical tachometer. The test rig was used to demonstrate the rotating motion of the wheel and the impact between the wheel and rail when the train operated. The whole test rig occupied a small space and was easy to handle; therefore, the experiments could be conducted in an anechoic chamber.

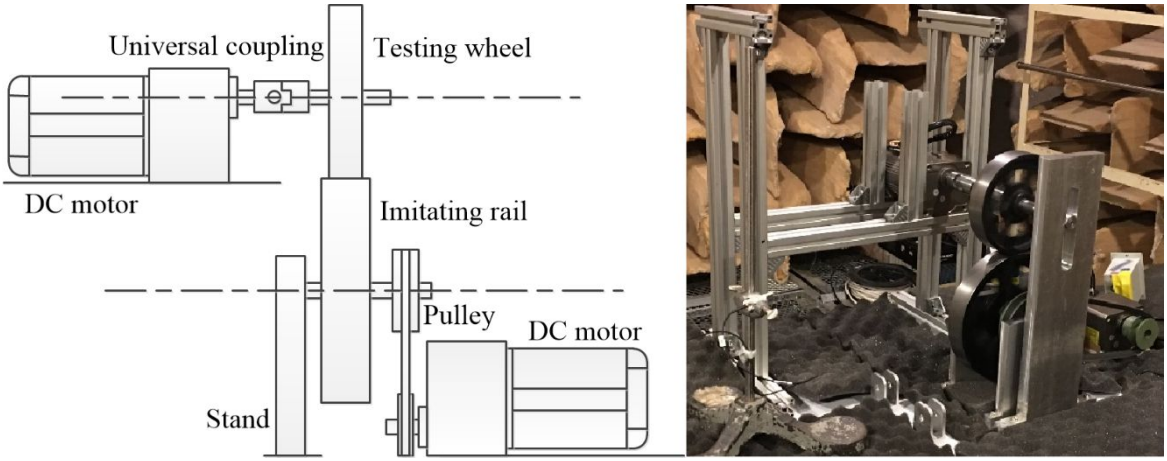

Fig. 4. Sketch and snapshot of roller test rig.

3.2 Identification of different types of faults

Three types of faults were created on the wheel to simulate the structural damages including dent, squat, and wheel-flat. Their snapshots and corresponding raw time-variant acoustic signals (in terms of voltage normalized by the maximum voltage) measured by one of the microphones when the two wheels were rotating together are shown in Fig. 5. Fig. 5(1a) shows the snapshot of the wheel without faults, while Fig. 5(2a), (3a), and (4a) show the snapshots of the wheel with the fault of dent, squat, and wheel-flat, respectively. Fig. 5 (3a) and (4a) show that the faults on the wheel surface are severe, and the impulsiveness of the signals in Fig. 5 (3b) and (4b) are obvious. However, it is difficult to distinguish between the signal of the dented wheel in Fig. 5 (2b) and that of the wheel without fault in Fig. 5 (1b)) by observation. To solve this problem, the kurtosis value is more appropriate to reflect the severity of the fault. This type of fault with less significant signals can be regarded as one of the early stage faults on the contact surfaces. To eliminate the potential safety issues, more efforts to conduct faults detection at the early stage should be performed.

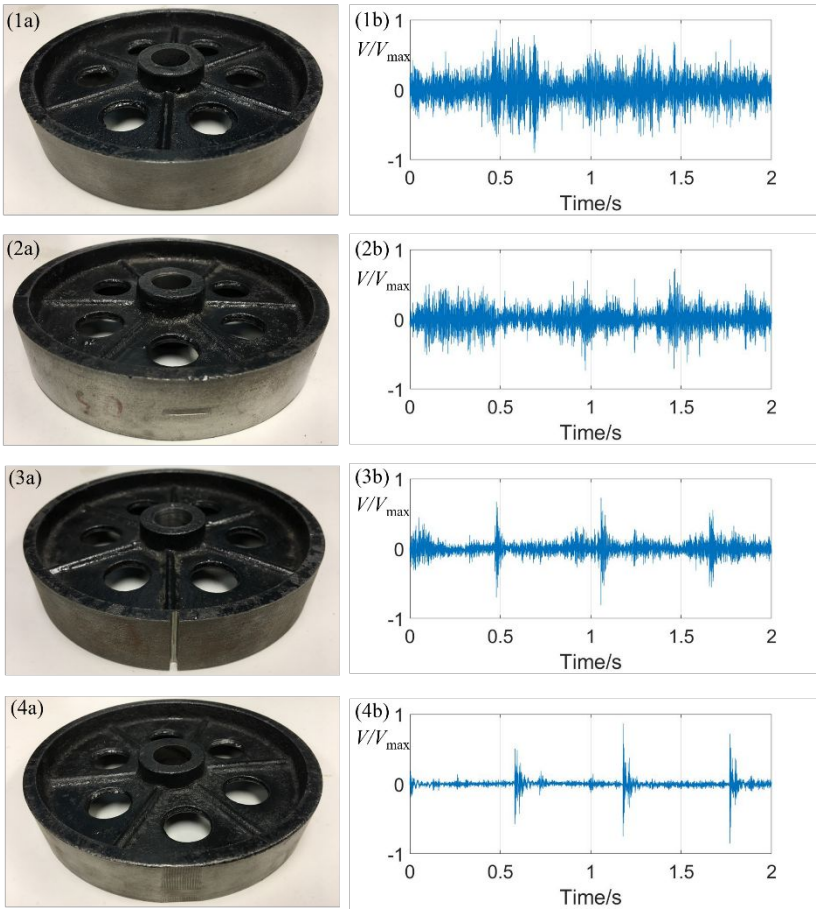

Fig. 5. Snapshots and time-domain signals of wheel without fault. (1a) snapshot of wheel without fault, (1b) signal of wheel without fault; (2a) snapshot of wheel with dent, (2b) signal of wheel with dent; (3a) snapshot of wheel with squat, (3b) signal of wheel with squat; (4a) snapshot of wheel with wheel-flat, (4b) signal of wheel with wheel-flat.

Different raw wheel fault signals with their kurtosis values are shown in Table 2. The measurements were repeated 20 times. To ascertain the fault level by the kurtosis value, a pure random noise signal from the loudspeaker, which was regarded as reference data, was generated for comparison and it yielded a kurtosis value of approximately 3. The first, second, and third columns of Table 2 indicate the fault type, kurtosis value, and standard deviation among all the tests, respectively. The fourth column indicates the relative sound pressure level (SPL) comparing the signals of the wheel

with faults with the signal of the wheel without fault. The rolling noise radiating from the wheel without fault yielded the kurtosis value of approximately 3.98, while that from the wheel with a 0.2-mm dent yielded the kurtosis value of approximately 4.5. This reflects that the small-sized dent, which cannot be identified from the time-variant data, can be recognised based on the kurtosis analysis. The kurtosis values of the squat and wheel-flat were significantly larger than that of the dent. Moreover, when the wheel faults were larger or became more serious, the kurtosis values became larger. Therefore, it is possible to determine the severity of the wheel faults and locate the faults using the kurtosis beamformer.

Table 2

Different types of wheel faults and their kurtosis values.

Type of signal	Kurtosis value	Standard deviation	Relative SPL (dB)
Random noise	3.0078	0.0128	N/A
Wheel without fault	3.9802	0.0342	+0.00
Dent (depth=0.2 mm)	4.5731	0.0686	+0.12
Dent (depth=0.5 mm)	4.6384	0.0497	+0.85
Dent (depth=2 mm)	4.2965	0.0629	+1.38
Squat	8.7016	0.3590	+2.09
Wheel-flat (depth=0.5 mm)	9.3195	0.4161	+2.75
Wheel-flat (depth=1 mm)	43.1276	2.3221	+4.92
Wheel-flat (depth=2 mm)	44.4229	1.2782	+7.91

3.3 Results of fault detection and localisation

Experiments were conducted to investigate the performance of time-domain beamforming integrated with kurtosis. All experiments were performed in an anechoic chamber with a background noise level of less than 15 dBA, and a cut-off frequency of 80 Hz to avoid sound reflections from the surrounding boundaries. Fig. 6 shows the experimental setup of the roller test rigs. A loudspeaker of diameter 9 cm was used to generate the background noise, while two roller test rigs that generated the impact noise and rolling noise were placed in the anechoic chamber. In the experiments, an array of sixteen microphones was aligned linearly with the microphone separation of 0.1 m. The array was placed 1.3 m above the floor and at 0.7 m perpendicular to the sound sources. The acoustic signals were captured by 16 Brüel & Kjær 9854 microphones, and amplified by a Brüel & Kjær Type 2694-A 16-channel DeltaTron conditioning amplifier. The analogue signals were converted into digital signals by four NI 9234 four-channel data acquisition cards.

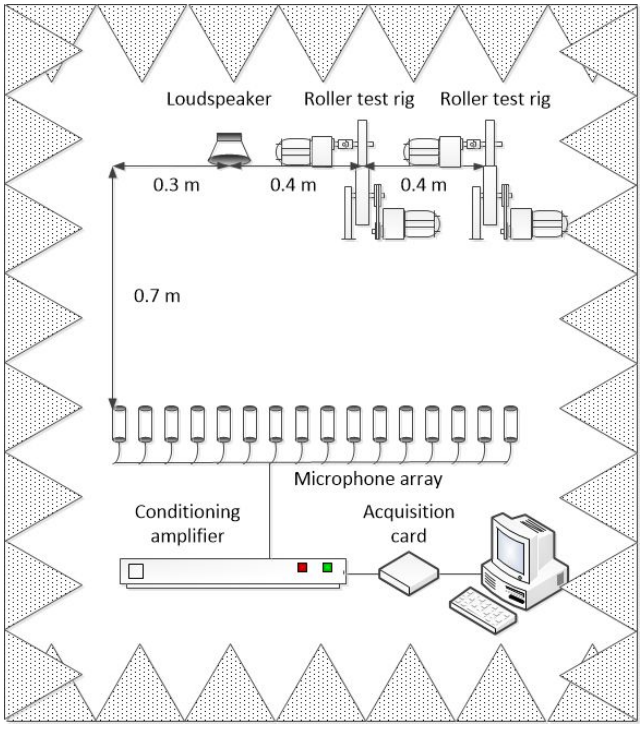

Fig. 6. Experimental setup of roller test rigs.

Fig. 7 shows the comparison between the result for the location of the fault by the traditional DAS beamformer, and that by the kurtosis beamforming. The roller test rig carrying a wheel with wheel-flat was installed at (0.7 m, 0.7 m), while another roller test rig carrying the wheel without fault was placed at (1.1 m, 0.7 m). Fig. 7(a) shows the time-domain beamforming power and Fig. 7(b) shows the time-domain kurtosis beamforming. Without the interference by the background white noise in this case, the location of the two sound sources due to the wheel system operation can be observed clearly in Fig. 7(a). The beamformer power at the location of the wheel without fault (square) is slightly less than that of the wheel with fault (diamond). Meanwhile, Fig. 7(b) shows that the kurtosis beamforming of the wheel with fault is significantly higher than that of the wheel without fault. This means that the sound map of the beamforming integrated with kurtosis is more effective at revealing the location of the wheel-flat and concealing the location of the normal wheel.

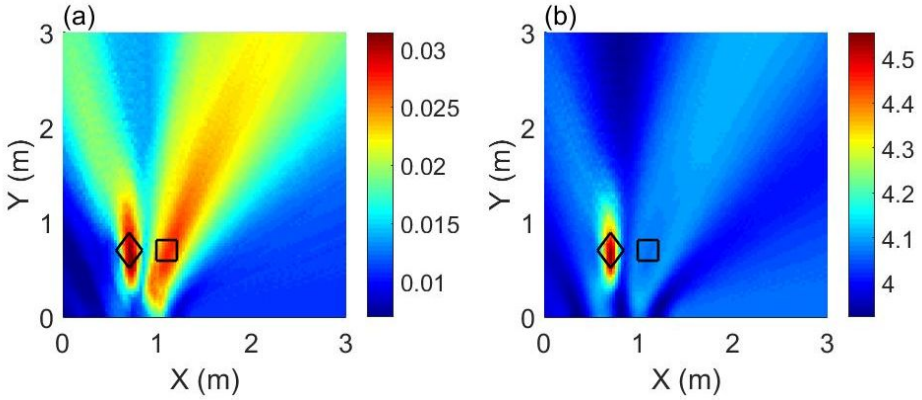

Fig. 7. Fault detection and localisation results of wheel with wheel-flat (◇: wheel-flat, and □: without fault). (a) DAS beamforming power, (b) kurtosis beamforming.

To further investigate the performance of the proposed method in the noisy environment, the effect of different SPL of background white noise was added; thus, a loudspeaker was placed at (0.3

m, 0.7 m) to generate a white noise. The first and second columns of Fig. 8 show the time-domain beamforming power and time-domain kurtosis beamforming, respectively. The first, second, and third rows of Fig. 8 show the localisation result of the wheel without fault and with the fault of dent, squat, and wheel-flat, respectively, under the background noise. In addition, the symbol of diamond, square, and circle show the actual location of the loudspeaker, the wheel without fault, and the wheel with fault, respectively. Fig. 8(1a) shows that the locations of the wheel with and without fault are vague, and it is difficult to identify these two types of sound sources. However, the location of the speaker appears to be clearer and identifiable from the sound map. This is primarily because of the SPL of background noise being higher than that of other two types of sound sources. Meanwhile, the location of the wheel with dent can be recognised approximately from the map of the kurtosis beamforming, as shown in Fig. 8 (1b), while the location of the speaker and the normal wheel cannot be identified. According to the literature, the size of roughly about 0.2 mm dent which is a fine depression at the rail surface is considered as an early stage of crack initiation and propagation[8]. In this regard, the kurtosis value 3.8 attributed to the dent with the same size which can reflect the early stage of faults on the wheel surface is considered as the baseline to determine the existence of the fault in the sound map. Similarly, Fig. 8(2a) and Fig. 8(3a) show a vague beamforming map; therefore, the location of the wheel with fault cannot be identified. Fig. 8(2b) shows a clear kurtosis beamformer map such that the location of the wheel with squat can be recognised. Fig. 8 (3b) depicts that the location of the wheel with the fault of wheel-flat is clear, and it is more acceptable than the dent and squat detections shown in Fig. 8 (1b) and (2b). This is because the kurtosis value of the dent is slightly larger than that of the wheel without fault; additionally, some sidelobes can be observed in Fig. 8 (1b).

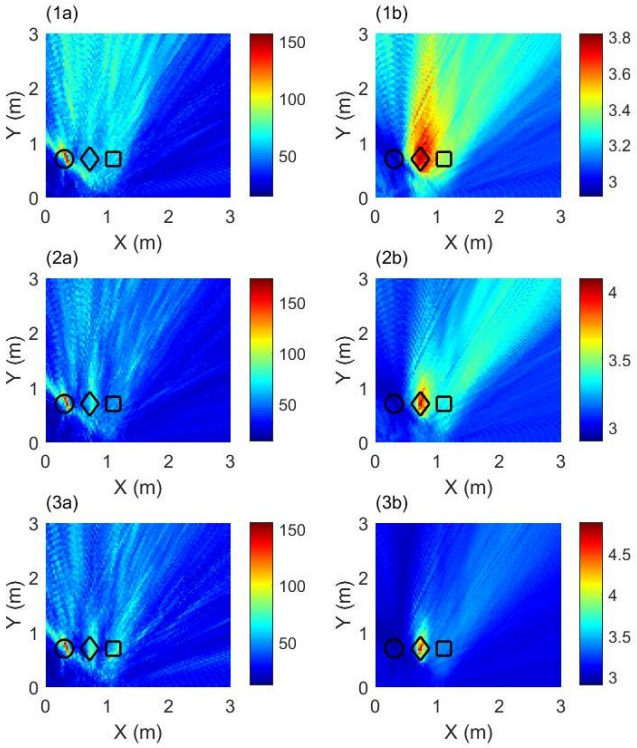

Fig. 8. Fault detection and localisation results (○: background noise, ◇: wheel with fault, and □: wheel without fault). (1a) DAS beamforming power of wheel with dent, (1b) kurtosis beamforming of wheel with dent; (2a) DAS beamforming power of wheel with squat, (2b) kurtosis beamforming of wheel with squat; (3a) DAS beamforming power of wheel with wheel-flat, (3b) kurtosis beamforming of wheel with wheel-flat.

Generally, kurtosis can be applied as a time-domain beamforming estimator to detect the impulsive signals generated by the impact of wheels with the fault in the wheel/rail system. Fig. 9 shows the comparison of the maps of the time-domain beamformer evaluated by different statistic estimators. The first, second, and third columns show the result of the RMS, peak value, and kurtosis value, respectively, for the localisation of the speaker, the pristine wheel and the wheel-flat. The second row of Fig. 9 shows the variation in amplitude of the corresponding beamforming estimator along the axial direction for Y=0.7 m. A study of the impulsive sound source localisation shows that the peak

value is better than the RMS as a statistic estimator to locate the sound source using the beamforming approach, owing to the achievement of a narrower beamwidth and a lower sidelobe level (SLL)[23]. In the present case of the localisation of an impulsive signal, the kurtosis value performed better than the peak, as observed in Fig. 9 (3b) and Fig. 9 (2b), respectively. The use of RMS estimation is to calculate the total sound power. Fig. 9 (1b) shows that the signal of the wheel-flat is weak with a low power level. Nevertheless, the kurtosis value is regarded as a better estimator to enhance the wheel-flat signal with respect to the background noise in Fig. 9 (3b). Consequently, kurtosis can be more advantageous than the RMS and peak value for the detection and localisation of a single impulsive sound source.

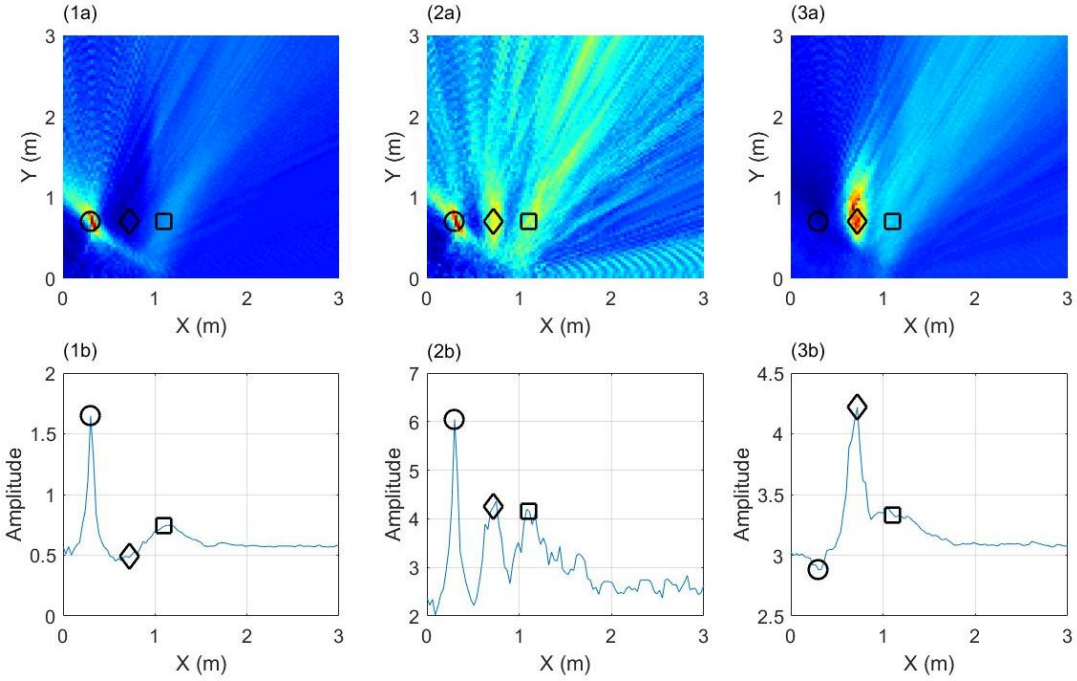

Fig. 9. Fault detection and localisation results using different statistic estimators (○: background noise, ◇: wheel with wheel-flat, and □: wheel without fault). (1a) RMS value, (1b) vertical view for RMS value at Y = 0.7 m; (2a) peak value, (2b) vertical view for peak value at Y = 0.7 m; (3a) kurtosis, (3b) vertical view for kurtosis at Y = 0.7 m.

3.4 Influence of signal-to-noise ratio and background noise

When the background noise is added in the sound field, it is difficult for the beamformer evaluated by RMS and peak value to identify the location of pristine wheel and the wheel-flat. It is noteworthy that in a real scenario or in the outdoor environment, the background noise may vary and thus may influence the accuracy of the fault identification of the railway wheel when using the kurtosis value. Therefore, the SPL of the loudspeaker was varied such that different SNRs were acquired by the array of microphones for analysis. Table 3 shows the result of the kurtosis value for different types of faults under different SNR ($SNR = Power_{fault} / Power_{background\ noise}$). The measurements were repeated 20 times. For each type of fault, the kurtosis values become smaller when the SNR is decreased. It is close to 3 when the SNR is too low, i.e., approximately 0.2 to 0.4 for the dent and squat, respectively. In this regard, the wheel may be misdiagnosed as a pristine structure without fault.

Table 3

Different SNRs applied to three types of faults signals and their kurtosis values.

Type of signal	SNR	Kurtosis value	Standard deviation
Dent (depth=2 mm)	0.6409	3.5003	0.0285
	0.4083	3.0380	0.0153
	0.1390	2.9848	0.0156
Squat	0.9236	5.9115	0.1198
	0.5884	4.3933	0.0577
	0.2003	3.1068	0.0165
Wheel-flat (depth=1 mm)	1.0934	30.9272	1.8299

	0.6965	11.1754	0.4175
	0.2371	5.4277	0.2417

Further investigations were conducted by comparing the localisation performance of the time-domain beamforming using the peak value, RMS, and kurtosis estimator under different SNRs. In this study, one loudspeaker generating different powers of random noise, located at (0.3 m, 0.7 m), and one roller test rig at (0.7 m, 0.7 m) were used. The SPL of background noise received by one of the microphones ranged from 35 dB to 98 dB when the roller test rig was switched off. Fig. 10 shows the beamforming map for the localisation of the wheel with the fault of wheel-flat under different SNRs. The first, second, and third column of Fig. 10 show the time-domain beamformer evaluated by the peak value, RMS, and kurtosis value, respectively. The first, second, third, fourth, fifth, and sixth row of Fig. 10 represent the beamforming map under the condition of background noise of approximately 84–98 dB, 72–83 dB, 66–71 dB, 60–65 dB, 55–59 dB, and 35–54 dB, respectively. In the experiments, the wheel-flat signal remained at 49 dB, and the background noise in the anechoic chamber was 26 dB. When the background noise is approximately 84–98 dB, the location of the speaker can only be observed based on the peak value in Fig. 10(1a) and the RMS in Fig. 10(1b). Additionally, the location of the wheel fault was totally merged even in the kurtosis beamformer map in Fig. 10(1c). Similar results of the beamformer output of peak and RMS values are shown in Fig. 10(2a) and Fig. 10(2b), respectively, when the background noise is approximately 72–83 dB. However, the location of the fault of wheel-flat can be approximately identified and localised using the kurtosis beamformer map, as shown in Fig. 10(2c). When the background noise is reduced to approximately 66–71 dB, both the location of the fault of wheel-flat and loudspeaker can be revealed using the RMS in Fig. 10(3b);

however, the loudspeaker location may be misdiagnosed as the fault. Meanwhile, the fault location can be recognised clearly using the kurtosis beamformer map as shown in Fig. 10(3c). When the background noise is further reduced to approximately 60–65 dB, the fault location can be localised by both beamformers of RMS and kurtosis, as shown in Fig. 10 (4b) and (4c), respectively. Moreover, the kurtosis beamformer performed better than the others owing to a lower SLL. When the background noise is reduced to 55–59 dB, the location of wheel-flat can be obtained by using the RMS and kurtosis. When the background noise is low, approximately 35–54 dB, such that white noise signal is buried in the signal of the wheel-flat, all the beamforming maps presented similar localisation results. It is noteworthy that the value of the kurtosis beamformer at the location of the wheel-flat gradually increases with the SNR. This is consistent with the result of Table 3. The kurtosis value has a positive correlation with the severity of faults and SNR.

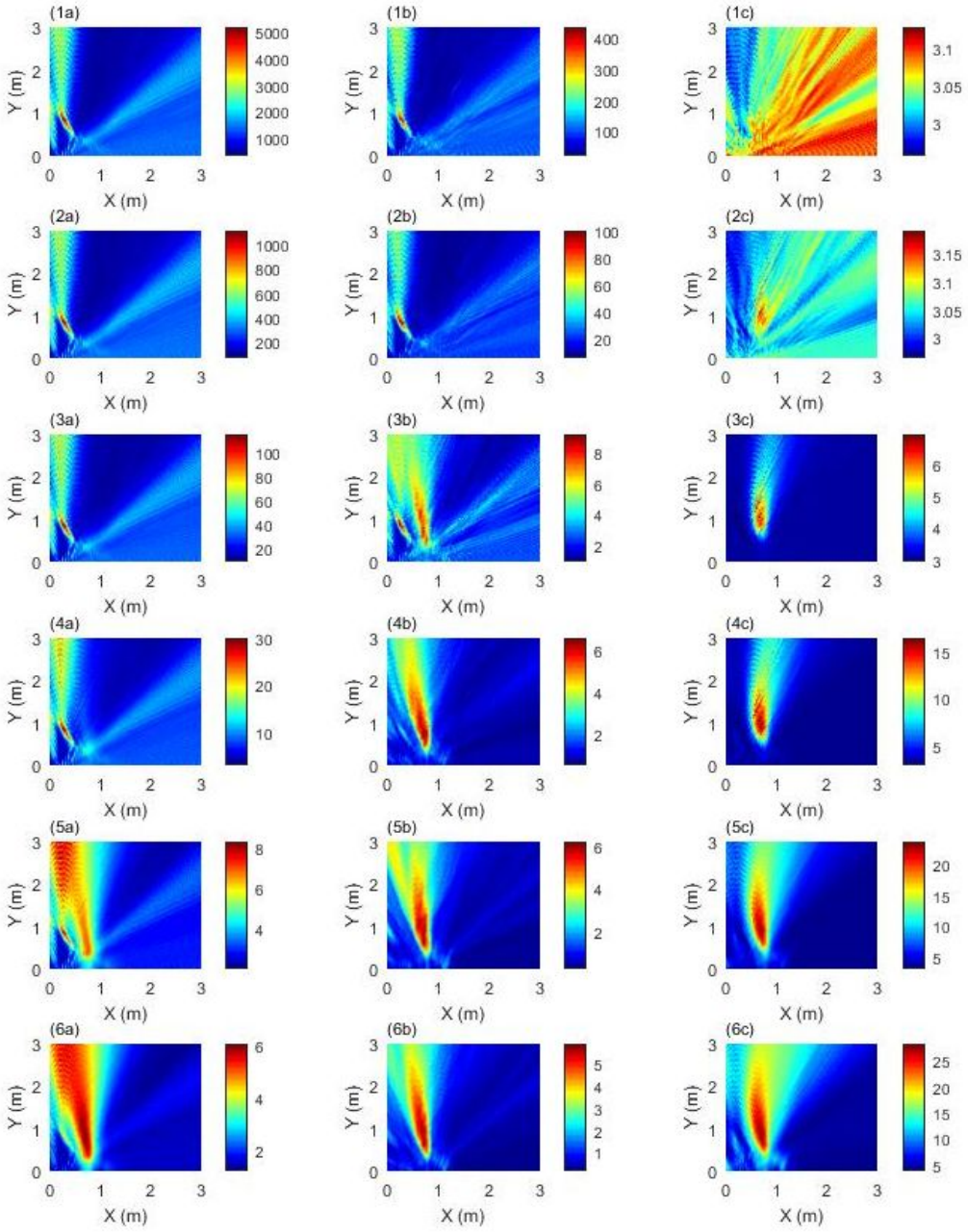

Fig. 10. Fault detection and localisation results using beamforming power, peak value, and kurtosis under different SNRs. The first, second, and third columns show the time-domain beamformer evaluated by peak, RMS, and kurtosis values, respectively. The first, second, third, fourth, fifth, and sixth row represent the beamforming maps under the background noise of approximately 84–98 dB, 72–83 dB, 66–71 dB, 60–65 dB, 55–59 dB, and 35–54 dB, respectively.

3.5 Influence of the duration of data acquisition on kurtosis value

The rotating wheel on the rail generates an impulsive signal comprising multiples impulses due to the multiple impacts when the train traverses on the rail. This raises a question: up to how many impulses can be contained for the detection? We assume that the impact noise generated is a Gaussian impulsive signal, such that

$$s(t) - = 2\pi^2 f^2 (t - 0.01n) e^{-2\pi^2 f^2 (t-0.01n)^2} \tag{10}$$

where f is the centre frequency, and n is a decay factor. In this case, f was set to be 100, while n was changed from 1 to 10. Fig. 11 shows the kurtosis value as a function of the number of impulses per second. The curve of the Gaussian impulsive signal has a similar trend with that of the measured data of the wheel-flat. When three impulses per second are adopted for the analysis, the kurtosis value can reach the maximum value of approximately 12. For the measured data of squat and dent, the kurtosis value can attain the maximum when the number of impulses per second is approximately 4. Generally, the kurtosis value could reach 6 or even higher when 1 to 10 impulses per second are used for the analysis. This indicates that when the duration of data acquisition for analysis contains at least one impulse signal, it would be accurate enough to identify the fault according to the kurtosis beamformer. However, if the number of impulses per second is high, the kurtosis value becomes low and may influence the accuracy of the fault localisation.

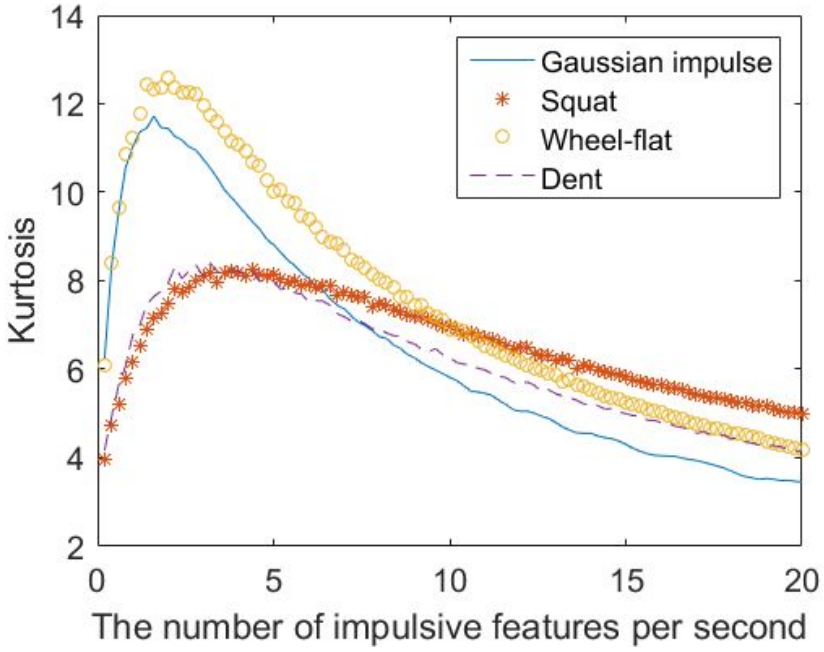

Fig. 11. Kurtosis values vs. the number of impulsive features per second in different signals.

3.6 Localisation of moving sound sources

This paper is focused on the fault detection of wheels in the wheel/rail system of a moving train. To mimic this scenario, the measurement and analysis of the moving sources will be shown. The function of kurtosis beamformer due to de-Dopplerisation is shown as follows:

$$Kurt(r_m) = \frac{E\{[b(\Delta \mathbf{r}_\kappa, \tau) - \mu(\Delta \mathbf{r}_\kappa, \tau)]^4\}}{[\sigma(\Delta \mathbf{r}_\kappa, \tau)]^4} \tag{11}$$

Fig. 12 shows the experimental setup of a moving track with three loudspeakers. The belt track simulates that the train is moving, and the loudspeakers are regarded as moving sound sources. Owing to limitation of space, it is difficult to conduct the experiment of the real railway system or movable wheel system in the anechoic chamber. Hence, the sound of the noise radiated from different types of faults from the wheel in the roller test rig was recorded and generated through the loudspeakers that were fixed on a movable trolley in the anechoic chamber.

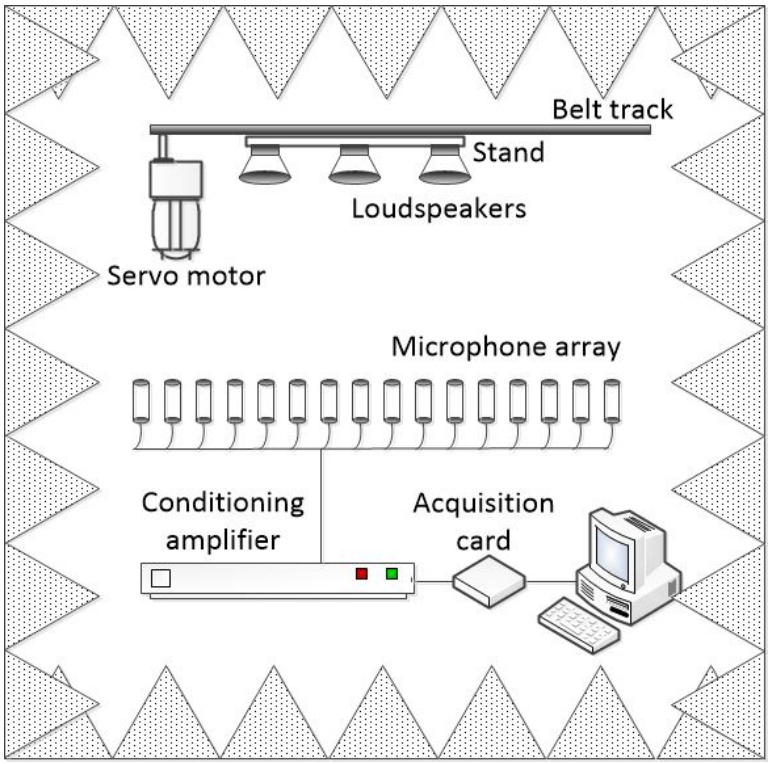

Fig. 12. Experimental setup of moving sound sources.

The purpose of this experiment is to examine the feasibility of locating the defect of the wheel/rail system when the trolley moves. The trolley moved at a speed of 0.2 m/s. Fig. 13 shows the kurtosis beamformer map of the detection and localisation for three moving sound sources. The symbols of circle, diamond, and square represent the location of the loudspeaker generating random noise, the sound of wheel with fault, and that of the wheel without fault, respectively. Fig. 13(1a) and (1b) show the beamformer evaluated by RMS and kurtosis, respectively, for the trolley that has moved after 2 s. Fig. 13(1a) shows that the location of the loudspeaker generating random noise can be revealed while the wheel with fault is marginally observed. This is primarily because the SPL of the background noise is set rather higher compared to the other two signals. Fig. 13(1b) shows that the speaker generating the wheel with fault can be recognised and is easier to be distinguished from the high background noise. Fig. 13(2a) and (2b) show the beamformer evaluated by RMS and kurtosis, respectively, for the

trolley that had moved after 4 s. Fig. 13(2b) shows that the location of the speaker generating the sound of the wheel with fault can be traced using the de-Dopplerisation and kurtosis beamforming approach. Although the present experimental test is limited to the speed of approximately 0.1 m/s to 0.5 m/s owing to the space issue, the results of Fig. 13 shows that the de-Dopplerisation and kurtosis beamforming approach are feasible to trace the wheel with fault.

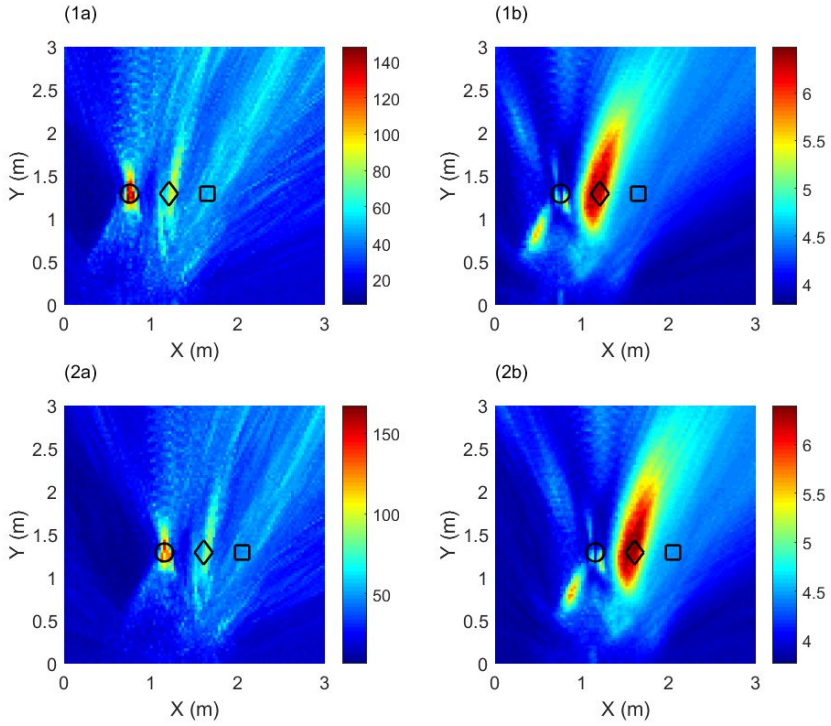

Fig. 13. Fault detection and localisation results for moving sound sources (○: background white noise, ◇: wheel with fault, and □: wheel without fault). (1a) DAS beamforming power at $\tau = 2\ s$, (1b) kurtosis beamforming at $\tau = 2\ s$, (2a) DAS beamforming power at $\tau = 4\ s$, (2b) kurtosis beamforming at $\tau = 4\ s$.

3.7 Comparison with current state-of-the-art approaches

In this section, the proposed kurtosis beamforming method is compared with current state-of-the-art approaches. The results are tabulated in Table 4. All the structural condition monitoring

approaches use non-destructive testing (NDT) techniques. In traditional vibration testing, accelerometers are mounted on the structure, and displacement and velocity are analysed with different frequency/time domain techniques. During this testing, the displacement and velocity of the structural component can easily be interfered by the vibration of the whole system. Magnetic or ultrasonic methods are a preferred solution to address this problem. Ultrasonic wave can travel over a long distance in materials with a high attenuation ratio, and be easily changed by damages or boundaries on its propagation path. Thus, it is suitable to detect faults in a large structure as well as recognize the different kinds of faults. In comparison with other traditional NDT techniques, Guided Lamb wave-based fault detection using piezoelectric lead zirconate titanate (PZT) elements, which is one of the most popular ultrasonic techniques, is considered cost-effective for use in applications. Unlike other detection methods, AE method is used to detect the transient elastic waves caused by crack formation. Therefore, it is more appropriate to investigate the dynamic behaviour of structures. In addition, this method is not employed to detect structural faults after the formation of faults. While all the structural crack detecting methods rely on waves propagating in the structures, as indicated in table 4, the kurtosis beamforming method relies on the acoustic waves propagating in the air, which is categorized as an acoustic imaging technique. The main advantage of this technique is that it eliminates the necessity to attach the sensors to the structure, making it suitable for a wide range of SNRs.

Table 4

Kurtosis beamforming method vs other condition monitoring approaches.

Condition monitoring approaches	Vibration technique	Ultrasonic technique	Magnetic methods	Acoustic emission	Kurtosis beamforming method
Actuators	Nil	Piezoelectric lead zirconate titanate elements	Ultrasonic control unit	Nil	Nil
Sensors	Accelerometers	Piezoelectric sensors	Electromagnetic acoustic transducer probes	Acoustic emission sensors	Microphones
Signal	Vibration signal	Lamb wave	Rayleigh wave	Transient elastic wave	Acoustic signal
Non-destructive testing	Yes	Yes	Yes	Yes	Yes
Estimating dynamic characteristics of faults	No	No	No	Yes	No
Requiring contact between sensors and structure	Yes	Yes	Yes	Yes	No

4. Conclusions

Herein, a hybrid approach integrating time-domain DAS beamforming with kurtosis for the identification and localisation of the fault of the wheel in a wheel/rail system was proposed. Its performance regarding the localisation of different types of faults of the wheel has been investigated

through experiments of stationary and moving sound sources. Different types of wheel faults can be identified according to the kurtosis value. The major conclusions are as follows:

1. By using de-Dopplerisation and the kurtosis beamforming approach, it is feasible to trace the location of the wheel with fault under the condition of high background noise. Additionally, different types of wheel faults such as dent, squat, and wheel-flat can be identified according to the kurtosis value.
2. Compared with the beamforming output evaluated by RMS and peak value, the kurtosis beamformer has a lower SLL and its ability to extract the impulsiveness emerging from the background noise is much stronger. Typically, the beamforming power can yield accurate positions of the sound sources in a field of multiple sound sources based on the acoustical power. When the background noise is high, the kurtosis outperforms the peak value and RMS to extract the feature of impulsive signals. In addition, the kurtosis value and its accuracy depended on the duration and number of impulses of the acquired signal for data analysis.
3. The influence of SNR on the kurtosis value for the signal of different types of faults has been investigated. The signals of significant faults with high SNRs tend to result in a large kurtosis value. Random noise or other interference distributions typically have a lower kurtosis value. However, the proposed method performs well when the fault is relatively small, where a low SPL or SNR is generated. Herein, the performance of the time-domain beamformer using three different estimators such as the peak, RMS, and kurtosis values under different SNR conditions has been studied. The kurtosis beamformer was found to be suitable for a wide range of SNRs, even in cases where the impulsive feature in the signal is completely indistinguishable using the traditional beamforming method from the background noise.

Acknowledgements

The work is supported and funded by the General Research Grant from the Hong Kong SAR government, (PolyU 5140/13E) and funding support from the Hong Kong Polytechnic University (Grant No: G-YBDL). We would like to acknowledge the encouragement from Prof. Jerome Antoni.

References

1. Alemi A, Corman F and Lodewijks G. Review on condition monitoring approaches for the detection of railway wheel defects.

2. Vér I, Ventres C and Myles M. Wheel/rail noise—part III: impact noise generation by wheel and rail discontinuities. *J Sound Vib* 1976; 46: 395-417.

3. Wang Y and Liang M. An adaptive SK technique and its application for fault detection of rolling element bearings. *Mech Syst Sig Process* 2011; 25: 1750-1764.

4. Liang B, Iwnicki S, Ball A, et al. Adaptive noise cancelling and time–frequency techniques for rail surface defect detection. *Mech Syst Sig Process* 2015; 54: 41-51.

5. Wu T and Thompson D. A hybrid model for the noise generation due to railway wheel flats. *J Sound Vib* 2002; 251: 115-139.

6. Grassie SL. Rail corrugation: advances in measurement, understanding and treatment. *Wear* 2005; 258: 1224-1234.

7. Grassie S and Kalousek J. Rail corrugation: characteristics, causes and treatments. *Proc Inst Mech Eng Part F-J Rail Rapid Transit* 1993; 207: 57-68.

8. Pal S, Daniel WJ and Farjoo M. Early stages of rail squat formation and the role of a white etching

layer. *Int J Fatigue* 2013; 52: 144-156.

9. Beebe RS. *Machine Condition Monitoring: How to Predict Maintenance Requirements for Rotating and Stationary Plant*. MCM Consultants, 1995.

10. Dornfeld D and Cai HG. An investigation of grinding and wheel loading using acoustic emission. *J Eng Ind* 1984; 106: 28-33.

11. Peng Z and Kessissoglou N. An integrated approach to fault diagnosis of machinery using wear debris and vibration analysis. *Wear* 2003; 255: 1221-1232.

12. Su Z, Ye L and Lu Y. Guided Lamb waves for identification of damage in composite structures: A review. *J Sound Vib* 2006; 295: 753-780.

13. Matsumoto A, Sato Y, Ohno H, et al. A new measuring method of wheel–rail contact forces and related considerations. *Wear* 2008; 265: 1518-1525.

14. Drinkwater BW and Wilcox PD. Ultrasonic arrays for non-destructive evaluation: A review. *NDT E Int* 2006; 39: 525-541.

15. Barke D and Chiu W. Structural health monitoring in the railway industry: a review. *Struct Health Monit* 2005; 4: 81-93.

16. Salzburger H-j, Schuppmann M, Li W, et al. In-motion ultrasonic testing of the tread of high-speed railway wheels using the inspection system AUROPA III. *Insight* 2009; 51: 370-372.

17. Zhang X, Feng N, Wang Y, et al. Acoustic emission detection of rail defect based on wavelet transform and Shannon entropy. *J Sound Vib* 2015; 339: 419-432.

18. Shibata K, Takahashi A and Shirai T. Fault diagnosis of rotating machinery through visualisation of sound signals. *Mech Syst Sig Process* 2000; 14: 229-241.

19. Lu W, Jiang W, Yuan G, et al. A gearbox fault diagnosis scheme based on near-field acoustic

holography and spatial distribution features of sound field. *J Sound Vib* 2013; 332: 2593-2610.

20. Fassois SD and Sakellariou JS. Time-series methods for fault detection and identification in vibrating structures. *Philosophical Transactions of the Royal Society of London A: Mathematical, Physical and Engineering Sciences* 2007; 365: 411-448.

21. Martin W. *The microprogrammable beamformer*. 1974. Technical Report, 1974. Raytheon Co.

22. Heilmann G, Meyer A and Döbler D. Time-domain beamforming using 3D-microphone arrays. *Proceedings of the BeBeC* 2008.

23. Seo D-H, Choi J-W and Kim Y-H. Impulsive sound source localization using peak and RMS estimation of the time-domain beamformer output. *Mech Syst Sig Process* 2014; 49: 95-105.

24. Wang Y, Xiang J, Markert R, et al. Spectral kurtosis for fault detection, diagnosis and prognostics of rotating machines: A review with applications. *Mech Syst Sig Process* 2016; 66: 679-698.

25. Cabada EC, Leclere Q, Antoni J, et al. Fault detection in rotating machines with beamforming: Spatial visualization of diagnosis features. *Mech Syst Sig Process* 2017; 97: 33-43.

26. Antoni J. The spectral kurtosis: a useful tool for characterising non-stationary signals. *Mech Syst Sig Process* 2006; 20: 282-307.

27. Kim Y-H and Choi J-W. *Sound visualization and manipulation*. John Wiley & Sons, 2013.